View metadata, citation and similar papers at core.ac.uk
brought to you by CORE
provided by Universidade do Minho: RepositoriUM

Vacuum 83 (2009) 1206–1212

Contents lists available at ScienceDirect

Vacuum

journal homepage: www.elsevier.com/locate/vacuum

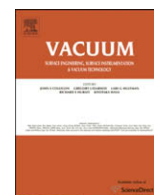

Structural evolution of Ti–Al–Si–N nanocomposite coatings

S. Carvalho [a], L. Rebouta [a,*], E. Ribeiro [a], F. Vaz [a], C.J. Tavares [a], E. Alves [b], N.P. Barradas [b], J.P. Riviere [c]

[a] Universidade do Minho, Departamento de Física, Azurém, 4800-058 Guimarães, Portugal
[b] ITN, Departamento de Física, E.N. 10, 2686-953 Sacavém, Portugal
[c] Laboratoire de Métallurgie Physique, Université de Poitiers, 86960 Futuroscope, France

Keywords:
Ti–Al–Si–N
Superhard nanocomposites
Solid solution hardening
Magnetron sputtering

A B S T R A C T

Ti–Si–Al–N films were prepared by rf reactive magnetron sputtering, in static and rotation modes, using a wide range of different deposition conditions, which created conditions to obtain Ti–Al–Si–N coatings with different structural arrangements.

Films prepared below a critical nitrogen flow, under conditions out of thermodynamic equilibrium, revealed a preferential growth of an fcc $(Ti,Al,Si)N_x$ compound with a small N deficiency. With nitrogen flow above that critical value, the reduction of the lattice parameter was no longer detected. However, a thermal annealing showed that a complete thermodynamically driven segregation of the TiN and Si_3N_4 phases was not yet obtained. The segregation upon annealing induced a self-hardening and showed a multiphase system, where the crystalline TiN, (Ti,Al)N and $(Ti,Al,Si)N_x$ phases were identified by X-ray diffraction. This behavior is due to the de-mixing of the solid solution associated to a small N deficiency.
© 2009 Elsevier Ltd. All rights reserved.

1. Introduction

In recent years, there has been increasing interest in nanostructured materials. The so-called nanocomposite films, consisting of nanocrystalline transition metal nitrides, MeN, and amorphous Si_3N_4 phase, which have unique mechanical, chemical and tribological properties, have been one of the most promising superhard materials. A wide variety of studies within this nanocomposite system, in particular in the nc-TiN/a-Si_3N_4, have been carried out during the last few years [1–10]. Al addition to these coatings showed promising results, improving the oxidation resistance, thermal stability and the performance in cutting tests [11–14]. When prepared under specific conditions, such as intense ion bombardment, high substrate temperature and high nitrogen activity, these coatings develop a two-phase system where nanocrystalline TiN grains are embedded in an amorphous silicon nitride matrix [1,2]. These conditions increase the thermodynamically driven segregation of TiN and Si_3N_4 phases, which is influenced by surface kinetics during deposition and thus, by the deposition temperature and especially ion bombardment conditions of the growing film (both influencing significantly the adatom mobility) [1,2,15]. The superhardness has its origin in the strong interface between TiN nanocrystallites and amorphous silicon nitride tissue. The hardness enhancement is achieved when TiN is covered with very thin silicon nitride tissues, corresponding to the percolation threshold of Si_3N_4 [16,17]. The interfaces prevent grain boundary sliding and dislocation propagation, contributing to the hardness enhancement [9,18].

The low temperature PVD deposition techniques are very popular and have been used to prepare this type of coatings. However, the low temperature introduces some kinetic constraints, which limit the phase formation to metastable ones. Ab initio calculations on the TiN–SiN system have shown that in case of some kinetic constraints, the formation of an fcc-$Ti_{1-x}Si_xN$ metastable phase occurs [19–21]. The same calculations allowed the calculations of the unit cell dimensions, and a similar lattice parameter values were obtained for $Ti_{1-x}Si_xN$ and TiN [19,20]. A cubic solid solution was already reported by other authors [4,22–24]. However, the small decrease of lattice parameter, when compared with the TiN one, is not in accordance with the calculated lattice parameter for the fcc-$Ti_{1-x}Si_xN$ metastable phase.

The purpose of this study is to present a comparative analysis of the structure of the samples and correlate them with different deposition parameters, in order to identify the nature of the phase with the reduced lattice parameter.

2. Experimental details

The films were deposited in a mixed Ar/N_2 atmosphere by rf reactive magnetron sputtering. A series of samples were produced in rotation mode, from high-purity Ti, Si and Al targets with the Ti and Si targets coupled to a rf source and the Al target coupled to a dc

* Corresponding author. Tel.: +351 2 5351 0472; fax: +351 2 5351 0461.
E-mail address: rebouta@fisica.uminho.pt (L. Rebouta).

0042-207X/$ – see front matter © 2009 Elsevier Ltd. All rights reserved.
doi:10.1016/j.vacuum.2009.03.009

power supply. In order to change the Si content, only the power applied to the Si target and the nitrogen flow were changed. A second series of samples were prepared in static mode from a Ti target with incrusted Al and Si pieces using rf power supply. The samples were deposited with substrate bias voltages and temperatures ranging from −25 V to −100 V and from 200 to 500 °C, respectively. Different discharge power and current combinations were used in the targets. The starting nitrogen partial pressure varied up to 6×10^{-2} Pa. Working pressures of 0.4 Pa were used during depositions. The films were deposited onto mechanically polished high-speed steel (AISI M2), austenitic steel (AISI 310), stainless steel (AISI 316) and mirror polished silicon (100) substrates.

Rutherford Backscattering Spectrometry (RBS) and Elastic Recoil Detection Analysis (ERDA) were used to access the atomic composition of the samples. Heavy ion ERDA experiments were done using a 40 MeV $^{35}Cl^{7+}$ beam in order to measure the concentration of light elements (carbon oxygen and nitrogen) in some samples. X-ray Photoelectron Spectroscopy (XPS) was used to analyze the chemical bonding status. The binding energy for the atomic level was calibrated for the value of carbon peak C 1s at 284.5 eV. X-ray diffraction (XRD) was used for structural characterization. Hardness measurements were performed in a Fischerscope H100, using maximum loads between 40 mN and 60 mN, depending on coating thickness. The corrections used in these measurements are described elsewhere [25]. The residual stresses were calculated using Stoney's equation [26] after measuring the curvature of the thin substrate (AISI 316) by laser triangulation, before and after deposition.

The thermal annealing was performed in a vacuum furnace with a base pressure of 10^{-4} Pa. The thermal cycle consisted of: 1 h heating up to the desired temperature, annealing for 1 h and free cooling in the furnace.

3. Results and discussion

3.1. Chemical composition

From composition analyses, the (Ti,Al,Si)N films used in this paper revealed Si contents varying between 0 and 13 at.%, Al contents in the range 8–19 at.% and N contents from 47 to 52 at.%. In the case of ERDA analysis (five samples), the Al and Si signals could only be separated down to a depth of around 100 nm. The total probed depth (for other elements such as Ti or N) was around 300 nm. Average film thickness was approximately 2 μm.

The oxygen contents in the five samples analyzed by ERDA are within the range 0.27–0.7 at.%. Accordingly with the conclusions of Veprek et al. [27] these values already decrease the achievable hardness. Three of the samples with 0.3 at.% of oxygen have hardness values higher than 40 GPa, while the other two samples (with oxygen contents of 0.4 and 0.7 at.%) revealed hardness values below 40 GPa.

3.2. Structure and lattice parameter

XRD patterns of samples prepared in rotation mode and deposited on 310 steel (except one deposited on M2 steel) are shown in Fig. 1. Although one peak is not enough to identify the film structure, using previous studies of other (Ti,Al,Si)N and (Ti,Si)N samples [28,29], it is possible to confirm the development of an fcc-type structure similar to that of δ-TiN in most of the samples. As an example, an XRD pattern of a (Ti,Al,Si)N sample deposited on an M2 steel is shown in Fig. 2a, where some peaks are clearly observed and can be assigned to the reflections from (111), (200), (220) and (311) planes of an fcc-type structure similar to that of δ-TiN. From those reflections a lattice parameter of 0.418 nm was calculated. The fcc-type structure was also confirmed by electron diffraction, as shown

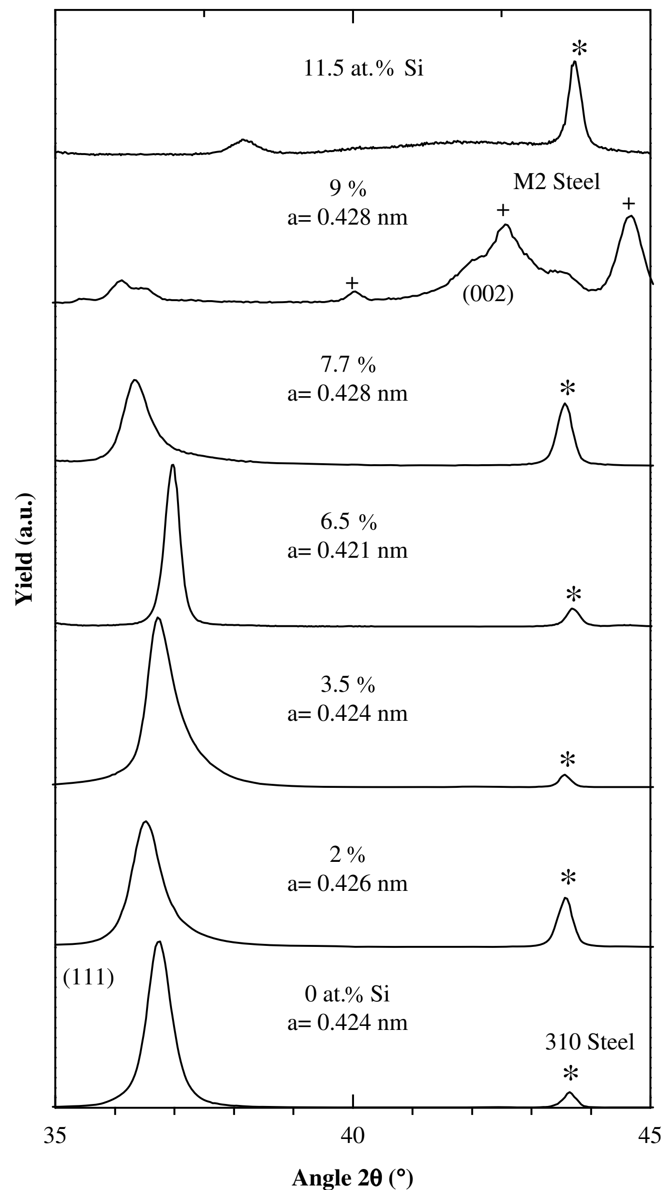

Fig. 1. XRD patterns of samples obtained in rotation mode with different Si contents (indicated in the figure).

in Fig. 2b. The Al content of the samples represented in Fig. 1 is between 14 and 18.5 at.%. The lattice parameter of the crystalline phases, calculated from XRD Bragg peaks, ranged from 0.419 to 0.429 nm. The (Ti,Al)N coating with 17.5 at.% of Al, revealed a lattice parameter of 0.424 nm, which agrees with results in literature, where a reduction in lattice parameter of about 0.004 nm was reported for this Al content [30,31]. The lattice parameter does not show any particular relation with Si contents, because samples with similar composition, for example between 8 and 10 at.% of Si and Al in the range 12–15 at.% revealed lattice parameters ranging from 0.419 to 0.429 nm and are the deposition parameters that play an important role. The residual stresses in these coatings are displayed in Fig. 3, as a function of the Si content. Although the deflection technique makes essentially an average evaluation on the whole volume of the coating (ordered and disordered domains) it gives a good evaluation of the grains' stress state [32]. All coatings revealed compressive stress states, which can be responsible for an increase of the lattice parameter, measured by conventional XRD, of about 1%. This means that the lattice parameters presented in this

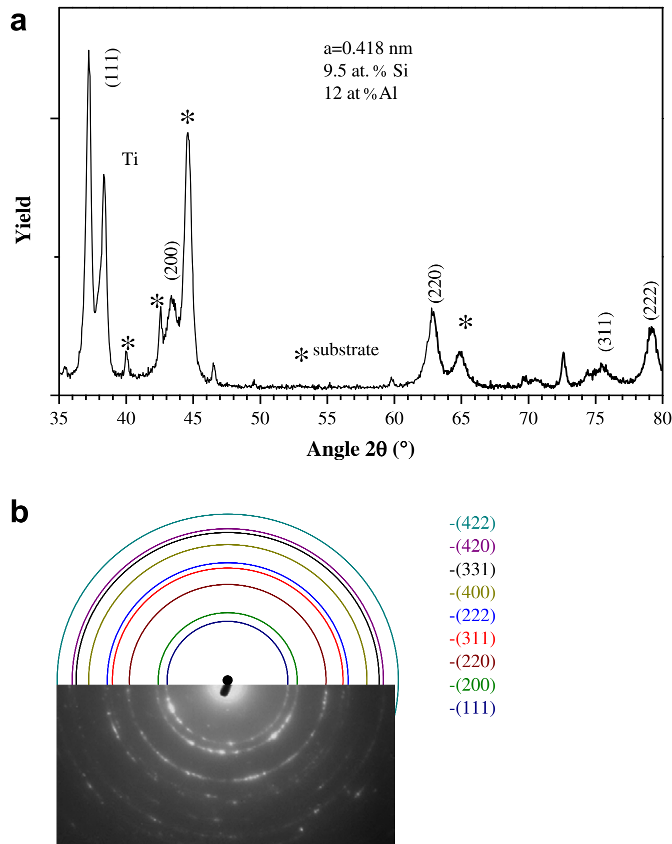

Fig. 2. a) XRD pattern of a (Ti,Al,Si)N sample deposited on an M2 steel, where some peaks are clearly observed and can be assigned to the reflections from an fcc-type structure similar to that of δ-TiN; b) electron diffraction pattern of the same sample.

paper are overestimated, when compared with the unconstrained ones, within a range of about 1%. The coatings with low Si content (<5 at.%) have very large compressive stress (>8 GPa), which decreases at higher Si contents. The development of the amorphous SiN phase is probably increasing with increasing Si content, which in turn, could be responsible for some stress relaxation phenomena, observed for these samples with the highest Si contents. The intensity decrease seen in the XRD patterns (Fig. 1) is associated with a decrease in the film crystallinity and/or film amorphization, which gives an indication of the possible amorphous SiN_x phase development.

In order to have a rough estimation of the nitrogen availability during the deposition, the ratio between nitrogen flow (cm^3/min) and deposition rate (nm/min) for the (Ti,Si,Al)N films prepared in static mode (rf-static series), using the same deposition chamber, was calculated according to this relation:

$$\text{nitrogen availability}(cm^3/nm) = \frac{\text{nitrogen flow}(cm^3/min)}{\text{deposition rate}(nm/min)}$$

This ratio, measured in cm^3/nm, gives better information on the nitrogen activity than the N_2/Ar flow ratio due to the target poisoning effect, which influences the deposition rate and also allows the comparison of samples prepared with different power applied to the target and with different nitrogen flow. The nitrogen activity is also influenced by other parameters, such as the substrate temperature and the ion bombardment rate.

In Fig. 4 the lattice parameter is displayed as a function of that ratio given in cm^3/nm. The Si content of each sample is indicated in the figure. In the case of samples prepared in rotation mode (Fig. 4a), the sample with the lowest lattice parameter was obtained with the lowest value of nitrogen availability parameter. For the case of the static mode series (Fig. 4b), there is also indication of some of the deposition parameters, like bias voltage, substrate

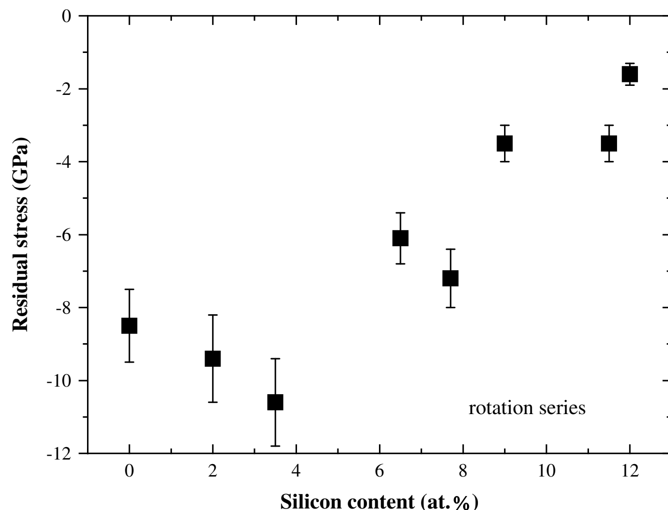

Fig. 3. Residual stress of the Ti–Si–Al–N samples obtained by rotation mode, as a function of the Si content.

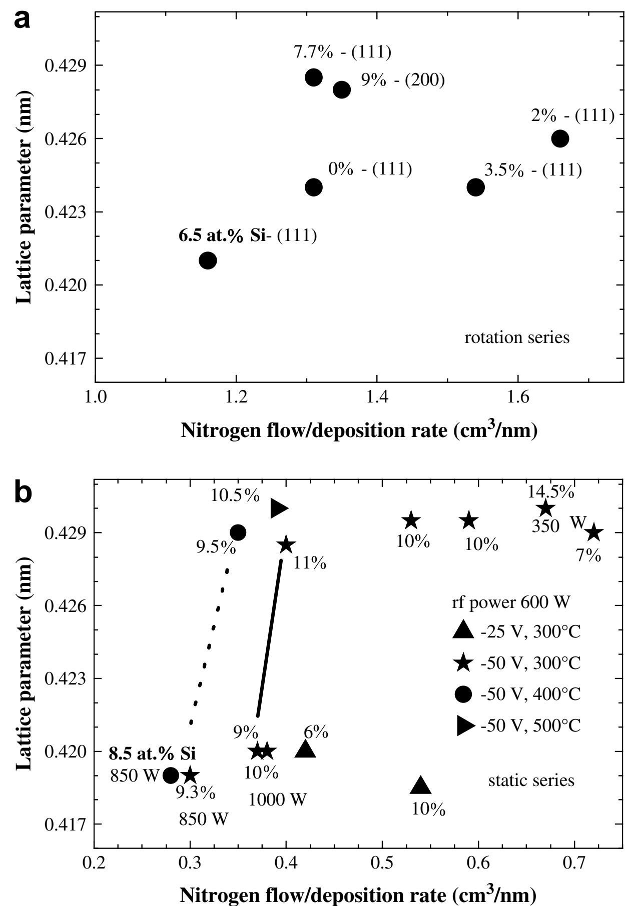

Fig. 4. Lattice parameter of the Ti–Si–Al–N samples prepared by rf sputtering in static mode as a function of nitrogen amount (nitrogen flow rate (cm^3/min)/deposition rate (nm/min)) used in its preparation: a) samples prepared in rotation and b) static mode series – the bias voltage, the substrate temperature and the rf power used in the preparation and the Si content of each sample is indicated in the graph.

temperature, and rf power applied to the target. From these results, it is possible to conclude that, keeping all the other parameters unchanged (bias voltage, substrate temperature, and argon pressure), below a critical nitrogen flow the formation of a structure with lower lattice parameter is favored. In these cases the substrate peak position did not show any shift.

The ERDA analysis of the one sample with a lattice parameter of 0.421 nm revealed a nitrogen content of 47.2 at.%, 0.71 at.% of oxygen and 1.2 at.% of carbon. However, another sample with a lattice parameter of 0.422 nm, revealed a nitrogen content of 51.2 at.%, 0.27 at.% of oxygen and 0.52 at.% of carbon. These compositions were obtained ignoring the thin surface oxide layer present in the surface films. The results are not conclusive, but suggest that the reduction of the lattice parameter can be related with some nitrogen deficiency and possibly with O and C impurities.

A similar shift of XRD peaks was also reported in the preparation of Ti–Si–N films by inductively coupled plasma assisted magnetron sputtering, synthesized at low deposition temperature (<150 °C) and irradiated with an high density low energy (~30 eV) ion flux (2 mA/cm^2) [33]. The films presented relatively low compressive residual stresses (<1.5 GPa), however, the XRD patterns revealed a gradual (200) peak shift to higher theta angles (lower lattice parameters) with the increase in Si content (from 2 to 11.3 at.% of Si) and with crystallite sizes higher than 20 nm, being ascribed to the TiN phase, although the correspondent lattice parameter is lower than that of unconstrained TiN.

An increase of the nitrogen flow above that critical value, leads to the formation of a phase with higher lattice parameter. In the critical region, an increase of either the substrate temperature (from 300 °C to 400 °C, with a bias voltage of −50 V) or the energy delivered to the substrate (bias voltage from −25 to −50 V, with a substrate temperature of 300 °C) increases the nitrogen activity, having the same effect on the lattice parameter. The samples prepared with a bias voltage of −25 V and a substrate temperature of 300 °C did not show any lattice parameter change with the nitrogen flow increase. In this case, the substrate temperature and the ion bombardment are not high enough, resulting in a low adatom surface mobility. This behavior can explain what seems a random dependence of the peak position and peak width on Si content of XRD patterns shown in Fig. 1. The samples were prepared using Ti, Al and Si targets and the Si content was augmented with an increase of the power applied to the Si target. The N flow was also increased, but in the some cases, as for example in the sample with 6.5 at.% of Si (Fig. 4a), the N flow increase did not follow the deposition rate increase. This resulted in lower nitrogen availability in the chamber and the sample revealed a peak position shift to higher theta angles.

Fig. 5 shows the XPS spectra of Si 2p signal for two (Ti,Al,Si)N samples having a similar Si content (6.5 and 6 at.%, respectively) but with different lattice parameters (0.421 and 0.428 nm, respectively). The spectra revealed that in these coatings the main signal (101.8 eV) is in agreement with the silicon fourfold coordinated to nitrogen as in Si_3N_4 [34]. A small oxygen contamination is also present. The 2p signals corresponding to the free Si and to the $TiSi_2$ phase were not found in the spectra, but a small amount cannot be excluded, being the behavior similar for both samples.

The increase in lattice parameter suggests the formation of the (Ti,Al)N and Si_3N_4 phases. The Si_3N_4 amorphous phase decreases the mobility of other atoms and limits the (Ti,Al)N grain growth. As a consequence, a reduction of the average crystallite size occurs, as seen in the nc-TiN/a-Si_3N_4 nanocomposite, where the average TiN grain size was found to decrease with increasing volume fraction of Si [1,2] using Fourier analysis [35]. The results are shown in Fig. 6 as a function of the lattice parameter. If deposition parameters are used according to the requirements reported by Veprek et al. [1,2], i.e. intense ion bombardment, high substrate temperature and high

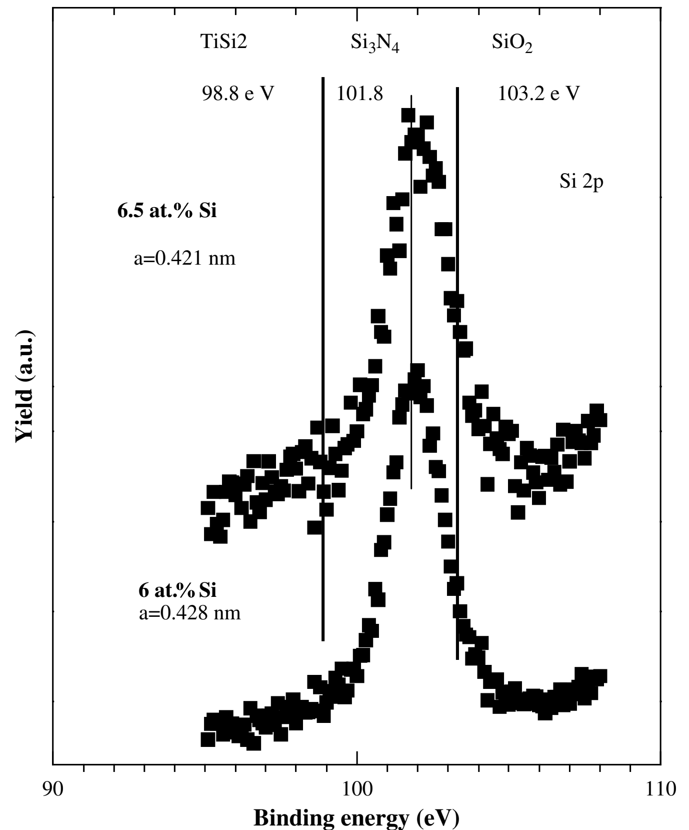

Fig. 5. XPS spectra of Si 2p signal for two (Ti,Al,Si)N samples having a similar Si content (6.5 and 6 at.%, respectively) but with different lattice parameters (0.421 and 0.428 nm, respectively).

nitrogen activity, the grain size would be strongly dependent on the volume fraction of the Si_3N_4 amorphous phase. On the contrary, with low deposition temperature, the grain size is not only determined by the Si content, but also strongly dependent on the deposition conditions, which induce thermodynamic and kinetic constraints and define the volume fraction of the amorphous phases. The samples that revealed the lowest lattice parameters (0.418–0.420 nm) have, in general, grain sizes higher than 15 nm. Grain sizes in the range 4–6 nm were obtained for lattice parameters between 0.427 and 0.429 nm, close to those of TiN. The ab initio

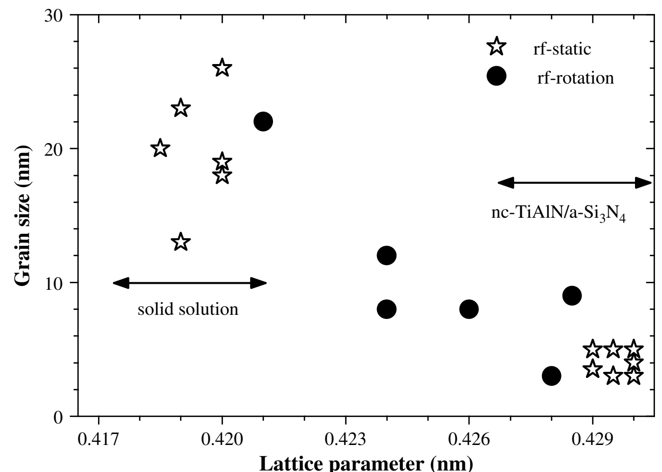

Fig. 6. Average crystallite size, obtained by Fourier analysis of X-ray Bragg reflections, as a function of the lattice parameter.

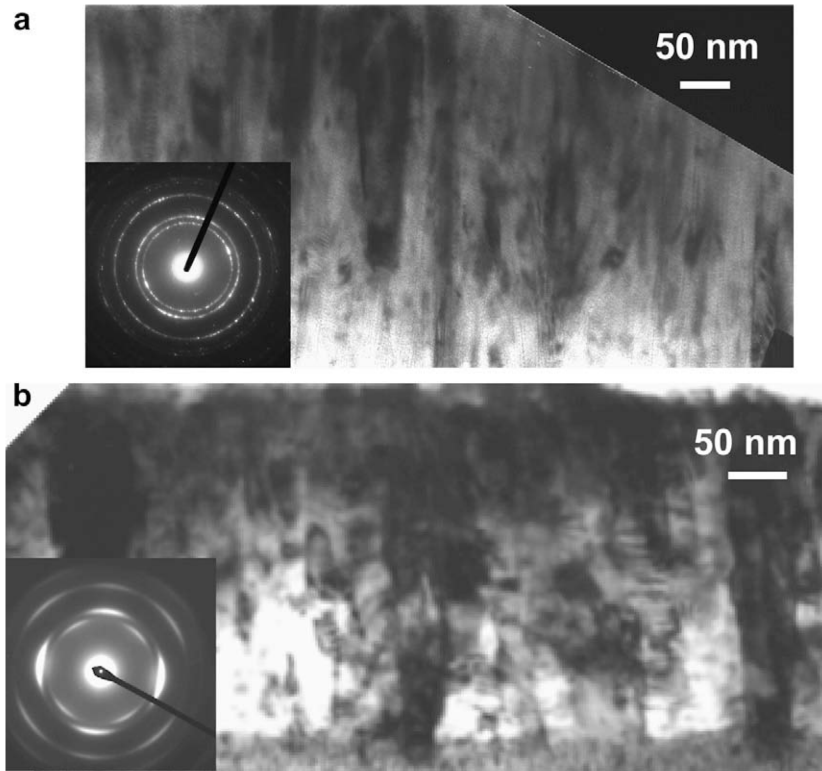

Fig. 7. Low magnification cross-sectional TEM micrographs of two samples prepared in rotation mode and with lattice parameters of 0.421 nm (a) and 0.428 nm (b).

calculations on the TiN–SiN system concluded that the fcc-$Ti_{1-x}Si_xN$ and TiN phases have a similar lattice parameter value [19,20]. From these calculations the phase with reduced lattice parameter cannot be attributed to fcc-$Ti_{1-x}Si_xN$. As mentioned, the XRD pattern of the phase with reduced lattice parameter was identified as an fcc B1 NaCl-type structure [4]. The N deficiency suggests that the Ti replacement by Si and Al in the fcc TiN_{1-x} lattice explains the low lattice parameter value for this metastable phase ($\sim$0.418 nm).

Fig. 7 shows low magnification cross-sectional TEM micrographs of two samples prepared in rotation mode and with lattice parameters of 0.421 nm (Fig. 7a) and 0.428 nm (Fig. 7b). Both show the presence of nanocrystalline columns in the growth direction, being more pronounced in the first sample. This also demonstrates that, due to the low deposition temperature and low nitrogen activity, a metastable phase is formed and the (Ti,Al)N grain growth inhibition does not occur. In the second case (Fig. 7b) the nitrogen activity was higher, but still not enough to induce the complete spinodal segregation of the (Ti,Al,Si)N metastable phase.

3.3. *Hardness thermal stability*

The variation of hardness as a function of the Si content for the series obtained in rotation mode is displayed in Fig. 8. A small increase was found with Si content, with the maximum obtained with the samples with 6.5 at.% of Si. This sample revealed a relatively high grain size and a lattice parameter of 0.421 nm, which indicates that the hardening mechanism can be related with solid solution and defect hardening.

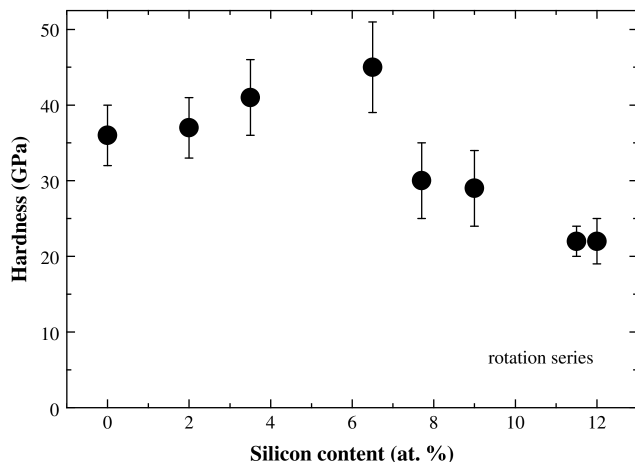

Fig. 8. Dependence of the hardness of Ti–Si–Al–N samples as a function of silicon content for the samples prepared in rotation mode.

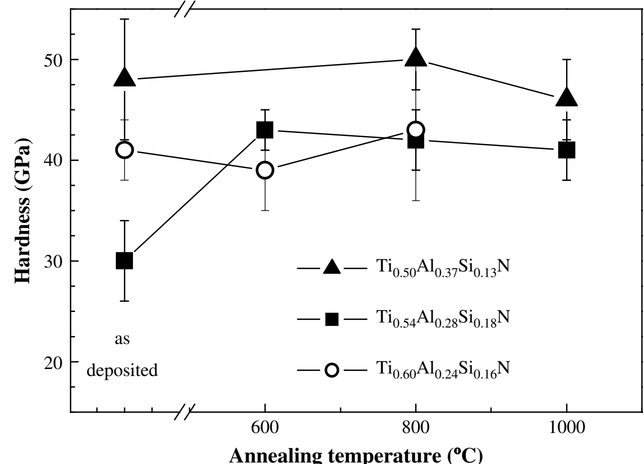

Fig. 9. Dependence of the hardness of the Ti–Si–Al–N samples in as deposited state and after thermal annealing in vacuum for 1 h at indicated temperatures.

Several samples were subjected to thermal annealing in vacuum in order to test both the structural evolution and the hardness retention with temperature increase. Those samples revealed three distinct behaviors and those behaviors are described in the hardness values evolution after the thermal annealing shown in Fig. 9 and in XRD patterns shown in Figs. 10–12. The first was the sample with 6.5 at.% of Si ($a = 0.421$ nm), and another with an average crystallite size of about 17 nm ($a = 0.423$ nm), both with a pronounced (111) texture, which revealed hardness values higher than 40 GPa. A third one ($Ti_{0.54}Al_{0.28}Si_{0.18}N$) is a sample with a small grain size (3 nm) and a lattice parameter of 0.430 nm ($H = 30$ GPa). The hardness of $Ti_{0.60}Al_{0.24}Si_{0.16}N$ and $Ti_{0.50}Al_{0.37}Si_{0.13}N$ samples has been retained after a thermal annealing at 1000 °C. On the other hand, $Ti_{0.54}Al_{0.28}Si_{0.18}N$ revealed a significant increase of hardness, from 30 to 43 GPa, after the annealing at 600 °C, keeping this value after the annealing at 1000 °C. These distinct behaviors can be understood with the analysis of the XRD patterns. The samples shown in Figs. 10 and 11 were deposited on M2 steel, while the last one was deposited on 310 steel. In order to distinguish the peaks from the substrate, are also shown in Figs. 10 and 12 the XRD patterns of substrates, as received and after the annealing in vacuum at 1000 °C. The as received 310 steel shows the characteristic peaks from austenitic phase (γ-Fe) and some peaks from carbide phases, which disappear after the annealing at 1000 °C, due to the high cooling speed. The XRD patterns of M2 steel reveal the peaks associated with the ferrite phase (α-Fe) and some primary carbides. Fig. 10 shows the XRD patterns at initial state and after thermal annealing at 800 °C and 1000 °C for the $Ti_{0.54}Al_{0.28}Si_{0.18}N$ film. The XRD patterns of the as deposited sample revealed a weak (200) texture. After the annealing at 800 °C and 1000 °C, three small peaks appeared in the region $2\theta = 36–37.5°$, with correspondence to peaks revealed in the region $2\theta = 42—43°$. Assuming an fcc-type structure, those peaks correspond to lattice parameters of 0.430 nm, 0.425 nm and 0.417 nm, respectively. These lattice parameters were identified as belonging to TiN, (Ti,Al)N and (Ti,Al,Si)N solid solution structures, respectively. This behavior suggests that thermodynamic segregation of TiN and Si_3N_4 phases was not complete, which means that a mixed phase is still present. The thermal annealing induced a spinodal decomposition, which was followed by a self-hardening.

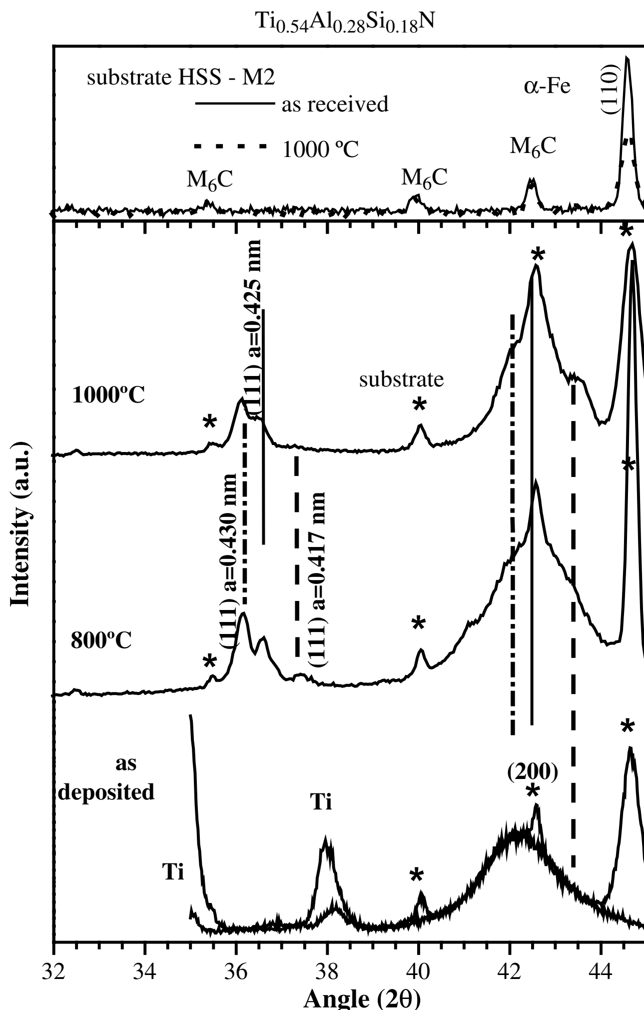

Fig. 10. X-ray pattern of the sample $Ti_{0.54}Al_{0.28}Si_{0.18}N$ in as deposited state and after thermal annealing in vacuum for 1 h at indicated temperatures.

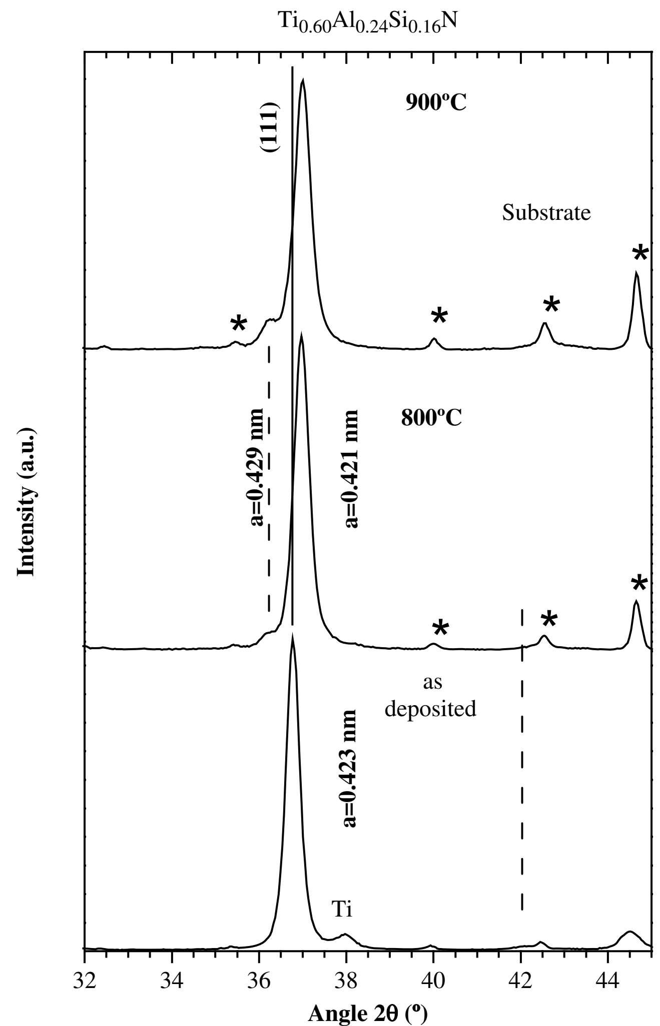

Fig. 11. X-ray pattern of the sample $Ti_{0.60}Al_{0.24}Si_{0.16}N$ in as deposited state and after thermal annealing in vacuum for 1 h at indicated temperatures.

The other two selected examples show a different behavior. The XRD patterns of $Ti_{0.60}Al_{0.24}Si_{0.16}N$ at initial state (Fig. 11) revealed a lattice parameter of 0.423 nm, which can be assumed as being (Ti,Al)N. With the thermal annealing a small decrease of the lattice parameter was found (0.421 nm), which can be explained by residual stress release. Additionally a small peak corresponding to TiN (0.429 nm) was revealed, although it could be already present in the as deposited sample, since it matches with the left tail of the main peak of the XRD pattern of the as deposited sample. After annealing, crystallization of the AlN phase was not found in this

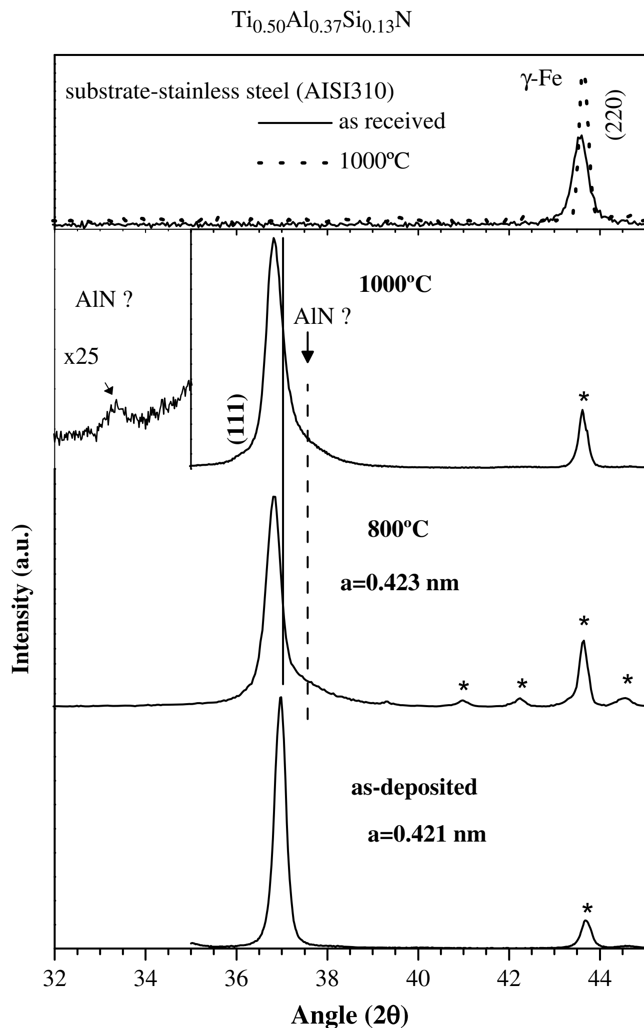

Fig. 12. X-ray pattern of the sample $Ti_{0.50}Al_{0.37}Si_{0.13}N$ in as deposited state and after thermal annealing in vacuum for 1 h at indicated temperatures.

sample, and the hardness retention suggests that (Ti,Al)N nanocrystallites are covered by the Si_3N_4 matrix, which avoids the high temperature decomposition of the (Ti,Al)N films, as reported in detail by Veprek et al. [11].

The XRD patterns of the third sample ($Ti_{0.60}Al_{0.24}Si_{0.16}N$) in the as deposited state, shown in Fig. 12, revealed a lower lattice parameter (0.421 nm), which slightly increased after thermal annealing at 800 °C, which is seen in a peak shift towards lower 2θ angle values. Additionally, at 1000 °C, the appearance of small peaks that are in good agreement with hexagonal AlN, suggests the spinodal decomposition of (Ti, Al)N, which was already observed by other authors after thermal annealing at 900 °C in (Ti,Al)N films [36]. Although the hardness values had revealed a slight decrease after annealing at 1000 °C, the eventual presence of the AlN phase suggests that nanostructure of the type nc-MeN/a-Si_3N_4 is not present. This behavior agrees with the presence of the solid solution, in this case with a lattice parameter similar to that expected for (Ti,Al)N. The decomposition occurs because the silicon nitride tissue is not enough to avoid the segregation of AlN. These results show that the different structural arrangements play different roles, contributing: (1) solid solution and defect hardening, (2) formation of a superhard nanocomposite of the type nc-MeN/a-Si_3N_4 or (3) formation of a multiphase system. These contributions explain the different behaviors for samples prepared in conditions that don't allow the spinodal segregation of the metastable phases.

4. Conclusions

Maintaining other deposition parameters unchanged (bias voltage, substrate temperature, and argon pressure), it was concluded that below a critical nitrogen flow, the formation of an fcc-(Ti,Al,Si)N metastable phase with a reduced lattice parameter is favored. The N deficiency suggests that the Ti replacement by Si and Al in the fcc-TiN_{1-x} lattice explains the low lattice parameter value for this metastable phase ($\sim$0.418 nm) and the relatively higher grain size when compared with samples with higher lattice parameter. The columnar growth presented in the samples also demonstrate that due to the low deposition temperature and low nitrogen activity a metastable phase is formed and the (Ti,Al)N grain growth inhibition does not occur.

An increase of the nitrogen flow above that critical value, leads to the formation of a phase with higher lattice parameter, but although revealing lower grain size, the nanocolumnar growth is still present, which indicates that the deposition conditions are still not enough to induce the complete spinodal segregation of the (Ti, Al, Si)N metastable phase.

References

[1] Veprek S, Reiprich S. Thin Solid Films 1995;268:64.
[2] Veprek S. Thin Solid Films 1998;317:449.
[3] Shizhi L, Yulong S, Hongrui P. Plasma Chem Plasma Process 1992;12:287.
[4] Vaz F, Rebouta L, Goudeau P, Girardeau T, Pacaud J, Riviére JP, et al. Surf Coat Technol 2001;146–147:274.
[5] Diserens M, Patscheider J, Lévy F. Surf Coat Technol 1999;120–121:158.
[6] Meng WJ, Zhang XD, Shi B, Tittsworth RC, Rehn LE, Baldo PM. J Mater Res 2002;17:2628.
[7] Nose M, Chiou WA, Zhou M, Mae T, Meshii M. J Vac Sci Technol 2002;A20:823.
[8] Hu X, Han Z, Li G, Gu M. J Vac Sci Technol 2002;A20:1921.
[9] Kong M, Zhao W, Wei L, Li G. J Phys D Appl Phys 2007;40:2858.
[10] Mannling HD, Patil DS, Moto K, Jílek M, Veprek S. Surf Coat Technol 2001;146–147:263.
[11] Veprek S, Männling HD, Jilek M, Holubar P. Mat Sci Eng 2004;A366:202.
[12] Veprek S, Jilek M. Vacuum 2002;67:443.
[13] Carvalho S, Ribeiro E, Rebouta L, Tavares C, Mendonça JP, Caetano Monteiro A, et al. Surf Coat Technol 2004;177–178:459.
[14] Nakonechna O, Cselle T, Morstein M, Karimi A. Thin Solid Films 2004;447–448:406.
[15] Hao S, Delley B, Stampfl C. Phys Rev B 2006;74:035424.
[16] Hao S, Delley B, Veprek S, Stampfl C. Phys Rev Lett 2006;97:086102.
[17] Veprek S, Reiprich S, Shizhi L. Appl Phys Lett 1995;66:2640.
[18] Söderberg H, Odén M, Molina-Aldareguia JM, Hultman L. J Appl Phys 2005;97:114327.
[19] Flink A, Larsson T, Sjolén J, Karlsson L, Hultman L. Surf Coat Technol 2005;200:1535.
[20] Zhang RF, Veprek S. Thin Solid Films 2008;516:2264.
[21] Zhang RF, Veprek S. Mat Sci Eng A 2007;448:111.
[22] Park I, Choi SR, Suh JH, Park C, Kim KH. Thin Solid Films 2004;447–448:443.
[23] Tanaka Y, Ichimiya N, Onischi Y, Yamada Y. Surf Coat Technol 2001;146–147:215.
[24] Carvalho S, Rebouta L, Cavaleiro A, Rocha LA, Gomes J, Alves E, et al. Thin Solid Films 2001;398–399:391.
[25] Antunes JM, Cavaleiro A, Menezes LF, Simões MI, Fernandes JV. Surf Coat Technol 2002;149:27.
[26] Stoney GG. Proc R Soc Lond Part A 1909;82:172.
[27] Veprek S, Männling HD, Niederhofer A, Ma D, Mukherjee S. J Vac Sci Technol B 2004;22:L5.
[28] Ribeiro E, Malczyk A, Carvalho S, Rebouta L, Fernandes JV, Alves E, et al. Surf Coat Technol 2002;151–152:515.
[29] Ribeiro E, Rebouta L, Carvalho S, Vaz F, Fuentes GG, Rodriguez R, et al. Surf Coat Technol 2004;188–189:351.
[30] Knotek O, Bohmer M, Leyendecker T. J Vac Sci Technol A 1986;4:2695.
[31] Ikeda T, Satoh H. Thin Solid Films 1991;195:99.
[32] Vaz F, Rebouta L, Goudeau Ph, Riviére JP, Schäffer E, Kleer G, et al. Thin Solid Films 2002;402:195.
[33] Li ZG, Moro M, Miyake S, Kumagai M, Saito H, Muramatsu Y. Surf Coat Technol 2005;193:345.
[34] Bischoff JL, Lutz F, Bolmont D. Surf Sci 1991;251–252:170.
[35] Mignot J, Rondot S. Acta Metall 1975;23:1321.
[36] Menzel S, Gobel T, Bartsch K, Wetzig K. Surf Coat Technol 2000;124:190.